High-frequency reflection and scattering of sound by ellipsoidally embossed surfaces

R. J. Lucas[a] and V. Twersky
Mathematics Department, University of Illinois, Chicago, Illinois 60680

(Received 7 October 1987; accepted for publication 11 January 1988)

Earlier results for coherent reflection and incoherent scattering by embossed rigid or free surfaces [V. Twersky, J. Acoust. Soc. Am. **29**, 209–225 (1957); **73**, 85–94 (1983)] are applied to ellipsoidal bosses with axes large compared to wavelength. The asymptotic procedures used originally for circular cylinders and spheres, and, subsequently, for elliptic cylinders [J. E. Burke and V. Twersky, J. Acoust. Soc. Am. **40**, 883–895 (1966)] are generalized to triaxial ellipsoids, and results for the corresponding bosses are obtained by the image method. Illustrative curves for both isotropic and anisotropic surfaces exhibit the influences of boss shape and orientation on the coherent reflection coefficients and incoherent differential scattering cross sections per unit area with emphasis on forward-(specular) and backscattered effects.

PACS numbers: 43.20.Fn

INTRODUCTION

In a previous article,[1] results[2,3] for scattering and reflection by relatively arbitrary bosses on rigid or free (pressure release) base planes were applied numerically to aligned ellipsoidal bosses with diameters small compared to wavelength (λ). Illustrative curves exhibited the low-frequency effects of boss shape and orientation on the coherent reflected intensity (R) and forward-scattered (specular) and backscattered cross sections per unit area [$\sigma(f)$ and $\sigma(b)$].

The present article provides high-frequency analogs for boss diameters large compared to wavelength. We use an asymptotic approximation[4] for scattering by a triaxial ellipsoid that includes the geometrically reflected term and the diffracted (shadow forming) term, and construct the required scattering amplitude for a single boss by the image procedure.[2,5] For the distribution of bosses, the corresponding results[2] for R and σ in terms of the isolated boss amplitude are mutually consistent in fulfilling the energy principle and account for coherent multiple scattering.

We consider both isotropic and anisotropic surfaces, and emphasize plots versus angle (α) of incidence (from the normal) for R, $\sigma(f)$, and $\sigma(b)$. Orientation effects are shown by plots with azimuthal angle (β) as the parameter. The graphs for broadside incidence ($\beta = 0$) are similar to those obtained for the striated case discussed earlier.[6] Closed form approximations for R and σ are included to indicate the dependence on parameters and to facilitate data inversion. Various illustrations and applications we consider were motivated by the programs of Diachok,[7] Roderick,[8] and others.

I. NOTATION

We write the position vector as

$$\mathbf{r} = r\hat{\mathbf{r}}(\theta,\varphi),$$
$$\hat{\mathbf{r}}(\theta,\varphi) = \sin\theta(\cos\varphi\,\hat{\mathbf{x}} + \sin\varphi\,\hat{\mathbf{y}}) + \cos\theta\,\hat{\mathbf{z}}, \tag{1}$$

and take the incident wave for a rigid (+) or free (−) base plane to be $\pm\phi' e^{-i\omega t}$, where

$$\phi' = \exp(i\mathbf{k}'\cdot\mathbf{r}), \quad \mathbf{k}' = k\hat{\mathbf{k}}', \quad k = 2\pi/\lambda,$$
$$\hat{\mathbf{k}}' = \hat{\mathbf{r}}(\pi - \alpha,\beta), \tag{2}$$

with $\hat{\mathbf{k}}'$ as the direction of incidence. The corresponding wave reflected from a smooth plane at $z = 0$ is the image

$$\phi = \exp(i\mathbf{k}\cdot\mathbf{r}), \quad \mathbf{k} = k\hat{\mathbf{k}}, \quad \hat{\mathbf{k}} = \hat{\mathbf{r}}(\alpha,\beta), \tag{3}$$

with $\hat{\mathbf{k}}$ as the direction of specular reflection. For brevity we define

$$\mathbf{s} = \hat{\mathbf{k}} - \hat{\mathbf{r}} \quad \text{and} \quad \mathbf{s}' = \hat{\mathbf{k}} - \hat{\mathbf{r}}. \tag{4}$$

When convenient, we work with the direction cosines

$$\hat{\mathbf{k}} = \gamma_x\hat{\mathbf{x}} + \gamma_y\hat{\mathbf{y}} + \gamma_z\hat{\mathbf{z}}, \tag{5}$$

with $\gamma_x = \sin\alpha\cos\beta$, $\gamma_y = \sin\alpha\sin\beta$, and $\gamma_z = \cos\alpha$.

For an ellipsoid centered at the orgin with principal semidiameters a, b, c along x, y, z, we write the dyadic[9] associated with the ellipsoid as

$$\tilde{\mathbf{E}} = \frac{\hat{\mathbf{x}}\hat{\mathbf{x}}}{a^2} + \frac{\hat{\mathbf{y}}\hat{\mathbf{y}}}{b^2} + \frac{\hat{\mathbf{z}}\hat{\mathbf{z}}}{c^2}, \tag{6}$$

so that $\mathbf{r}\cdot\tilde{\mathbf{E}}\cdot\mathbf{r} = 1$ is the equation of the ellipsoid. The use of $\tilde{\mathbf{E}}$ and its reciprocal

$$\tilde{\mathbf{E}}^{-1} = a^2\hat{\mathbf{x}}\hat{\mathbf{x}} + b^2\hat{\mathbf{y}}\hat{\mathbf{y}} + c^2\hat{\mathbf{z}}\hat{\mathbf{z}}, \tag{7}$$

such that $\tilde{\mathbf{E}}\cdot\tilde{\mathbf{E}}^{-1} = \tilde{\mathbf{I}}$ is the identity, leads to simple forms for factors that arise in the development.

We let $g(\hat{\mathbf{r}},\hat{\mathbf{k}})$ denote the scattering amplitude for ϕ incident on an ellipsoid at the phase origin. The scattering amplitude for the corresponding boss on a rigid or free base plane excited by $\pm\phi'$ follows by superposition[2]

$$f_\pm(\hat{\mathbf{r}},\hat{\mathbf{k}}') = g_\pm(\hat{\mathbf{r}},\hat{\mathbf{k}}) \pm g_\pm(\hat{\mathbf{r}},\hat{\mathbf{k}}'). \tag{8}$$

The coherent reflected field, the ensemble averaged wave for the base plane plus bosses, has the form[2]

$$\phi(1 + Z)/(1 - Z), \quad Z = \pi n f(\hat{\mathbf{k}},\hat{\mathbf{k}}')/k^2\cos\alpha, \tag{9}$$

[a] Visiting from the Department of Mathematical Sciences, Loyola University, Chicago, IL 60626.

 0001-4966/88/062005-07$00.80

where n is the average number of bosses in unit area. As before, we suppress subscripts $\pm$ where feasible.

The coherent power reflection coefficient equals[2]

$$R = |(1 + Z)/(1 - Z)|^2, \tag{10}$$

and the incoherent scattering in a direction $\hat{\mathbf{r}}$ is specified by the differential scattering cross section per unit area[2]:

$$\sigma(\hat{\mathbf{r}},\hat{\mathbf{k}}') = (n/k^2)|f(\hat{\mathbf{r}},\hat{\mathbf{k}}')/(1 - Z)|^2. \tag{11}$$

Energy conservation for lossless bosses is exhibited by (10) and (11) in that the total scattering from unit area, the integral of (11) over the observer's half-space of directions, satisfies[2]

$$(1 - R)\cos\alpha = \int \sigma(\hat{\mathbf{r}},\hat{\mathbf{k}}')d\Omega(\hat{\mathbf{r}}). \tag{12}$$

Although more complete forms are available in terms of the statistical mechanics pair correlation function,[3] these simple forms for sparse distributions appear appropriate for the applications in view.[7,8] As discussed before,[6] for some purposes a single scattering approximation may be better except near grazing incidence.

II. LARGE ELLIPSOIDAL BOSSES

For an ellipsoid whose semidiameters are large compared to wavelength, a Kirchhoff (tangent plane) approximation in the surface integral representation of g suffices for the essentials. As before,[2,4] for rigid (+) or free (−) surfaces, we obtain a geometrically reflected term g_1 and a diffracted (shadow forming) beam g_2:

$$g_\pm(\hat{\mathbf{r}},\hat{\mathbf{k}}) = g_2(\hat{\mathbf{r}},\hat{\mathbf{k}}) \pm g_1(\hat{\mathbf{r}},\hat{\mathbf{k}}),$$

$$g_{1,2} = -\frac{k^2}{4\pi}\int_{1,2} e^{ik\boldsymbol{\rho}\cdot(\hat{\mathbf{k}} - \hat{\mathbf{r}})}\hat{\nu}\cdot(\hat{\mathbf{k}} \mp \hat{\mathbf{r}})ds(\boldsymbol{\rho}). \tag{13}$$

Here, $\boldsymbol{\rho}$ is the radius vector to a point on the ellipsoid's surface and $\hat{\nu}$ is the normal. The subscripts 1 and 2 indicate integration over the irradiated and shadowed sides of the ellipsoid; the planar curve $\hat{\mathbf{k}}\cdot\hat{\nu} = 0$ corresponds to the shadow boundary.

The integral over the irradiated side may be evaluated by the method of stationary phase (except near the forward direction). Thus, in terms of the principal radii of curvature ρ_1 and ρ_2 at the point of reflection $\mathbf{r}_s$,

$$g_1(\hat{\mathbf{r}},\hat{\mathbf{k}}) = ike^{ik\mathbf{s}\cdot\mathbf{r}_s}(\rho_1\rho_2/2) = ik(abc/2)De^{-ikP},$$

$$P^2 = \mathbf{s}\cdot\tilde{\mathbf{E}}^{-1}\cdot\mathbf{s}, \quad D = \mathbf{s}\cdot\mathbf{s}/P^2. \tag{14}$$

The form for g_1 exhibited in (14) is not valid near the forward direction ($\hat{\mathbf{r}} \approx \hat{\mathbf{k}}$) where the method of stationary phase breaks down. Near the forward direction we expand the integrand as a Taylor series and integrate the first two terms exactly to obtain

$$g_1(\hat{\mathbf{r}},\hat{\mathbf{k}}) \sim (k^2abc/4\Gamma)\mathbf{Q}\cdot\mathbf{s} - ik^3(abc/6)(\mathbf{s}\cdot\mathbf{s});$$
$$\mathbf{Q} = \hat{\mathbf{k}}\cdot\tilde{\mathbf{E}},$$
$$\Gamma^2 = \hat{\mathbf{k}}\cdot\tilde{\mathbf{E}}\cdot\hat{\mathbf{k}} = (\Delta\sin\alpha)^2 + (\cos\alpha)^2/c^2, \tag{15}$$
$$\Delta^2 = (\sin\beta)^2/b^2 + (\cos\beta)^2/a^2,$$
$$\mathbf{s}\cdot\mathbf{s} = 2(1 - \hat{\mathbf{k}}\cdot\hat{\mathbf{r}}).$$

Thus, although (14) need not vanish for $\hat{\mathbf{r}} \to \hat{\mathbf{k}}$, the appropriate form (15) vanishes in the limit. In particular, for $\varphi = \beta$, and $\alpha = \pi/2 - \tau$, $\tau \approx 0$ (corresponding to near-grazing incidence and observation in the specular direction for the boss),

$$g_1(\hat{\mathbf{k}},\hat{\mathbf{k}}') \sim k^2\tau ab(1 - 4ik\Delta c^2/3)/(2c\Delta). \tag{16}$$

The integral for g_2 may be evaluated exactly[4] in terms of the Bessel function J_1. Using Green's theorem, we replace the surface of integration by the elliptic disk that closes the shadowed side of the ellipsoid, i.e., by the disk defined by the shadow boundary $\hat{\mathbf{k}}\cdot\hat{\nu} = 0$:

$$\mathbf{r}\cdot\tilde{\mathbf{E}}\cdot\hat{\mathbf{k}} = \frac{x\gamma_x}{a^2} + \frac{y\gamma_y}{b^2} + \frac{z\gamma_z}{c^2} = 0. \tag{17}$$

Thus, if $\mathbf{L}_1$ and $\mathbf{L}_2$ are the directed semidiameters of the disk, then

$$g_2(\hat{\mathbf{r}},\hat{\mathbf{k}}) = -(k^2abc/2\Gamma)(\hat{\mathbf{r}} + \hat{\mathbf{k}})\cdot\mathbf{Q}J_1(U)/U,$$
$$U^2 = k^2[(\mathbf{L}_1\cdot\mathbf{s})^2 + (\mathbf{L}_2\cdot\mathbf{s})^2]. \tag{18}$$

For the triaxial ellipsoid we write

$$\mathbf{L}_i = L_i\hat{\mathbf{L}}_i = L_i(\ell_i\hat{\mathbf{x}} + m_i\hat{\mathbf{y}} + n_i\hat{\mathbf{z}}), \quad i = 1,2, \tag{19}$$

where the semidiameters are given by[10]

$$L_i^2 = [B \pm (B^2 - 4AC)^{1/2}]/2A,$$
$$A = \hat{\mathbf{k}}\cdot\tilde{\mathbf{E}}\cdot\hat{\mathbf{k}}, \quad B = (a^2 + b^2 + c^2)A - 1, \tag{20}$$
$$C = (abc)^2\hat{\mathbf{k}}\cdot\tilde{\mathbf{E}}\cdot\tilde{\mathbf{E}}\cdot\hat{\mathbf{k}}.$$

Their orientations are expressed in terms of the direction cosines[10]

$$\ell_i = \gamma_x(r_i^2 - b^2)(r_i^2 - c^2)/d_i,$$
$$m_i = \gamma_y(r_i^2 - a^2)(r_i^2 - c^2)/d_i, \tag{21}$$
$$n_i = \gamma_z(r_i^2 - a^2)(r_i^2 - b^2)/d_i,$$

with $r_i = L_i$, and

$$d_i^2 = [\gamma_x(r_i^2 - b^2)(r_i^2 - c^2)]^2 + [\gamma_y(r_i^2 - a^2)(r_i^2 - c^2)]^2 + [\gamma_z(r_i^2 - a^2)(r_i^2 - b^2)]^2.$$

In particular, for incidence in the xz plane ($\beta = 0°$, corresponding to broadside incidence at grazing if $b > a$),

$$\mathbf{L}_1 = b\hat{\mathbf{y}}, \quad \mathbf{L}_2 = (a^2/d)\cos\alpha\,\hat{\mathbf{x}} - (c^2/d)\sin\alpha\,\hat{\mathbf{z}},$$
$$d = (a^2\cos^2\alpha + c^2\sin^2\alpha)^{1/2}, \tag{22}$$
$$U^2 = k^2\{b^2\sin^2\theta\sin^2\varphi + [a^2\cos\alpha(\sin\alpha - \sin\theta\cos\varphi) - c^2\sin\alpha(\cos\alpha - \cos\theta)]^2/d^2\}.$$

For incidence in the yz plane ($\beta = 90°$, nose-on incidence for $b > a$), we obtain $\mathbf{L}_i$ and U from the above by interchanging $\hat{\mathbf{x}}$ and $\hat{\mathbf{y}}$, a and b, as well as $\sin\varphi$ and $\cos\varphi$. If $a = b$, then (22) corresponds to the spheroid with symmetry axis along $\hat{\mathbf{z}}$. If $a = b = c$, then U reduces to the form obtained earlier[2] for the sphere,

$$U = ka[1 - (\hat{\mathbf{r}}\cdot\hat{\mathbf{k}})^2]^{1/2}. \tag{23}$$

Substituting (13), (14), and (18) into f of (8), we write Z of (9) as

$$Z_{\pm} = -\frac{wc\Gamma}{2\cos\alpha}\left(1 \pm \frac{\Delta^2 \sin^2\alpha\, J_1(2ku\cos\alpha)}{k\Gamma^2 u\cos\alpha} - \frac{ie^{-2ikc\cos\alpha}}{kc^2\Gamma}\right),$$

$$u = [(\mathbf{L}_1\cdot\hat{\mathbf{z}})^2 + (\mathbf{L}_2\cdot\hat{\mathbf{z}})^2]^{1/2} = [(L_1 n_1)^2 + (L_2 n_2)^2]^{1/2}, \tag{24}$$

where $w = n\pi ab$ (the packing fraction) is the fraction of the base plane covered by bosses.

III. SPECIAL CASES

As discussed previously for hemispherical bosses,[2] the first term of Z of (24) (the shadow term arising from the image wave) is the largest; the second (the shadow term of the incident wave) is negligible except near grazing. The third term (the incident wave reflected at the curved surface) indicates specular reflection at the tangent plane of the bosses. This term is significant in the reflection coefficient when $wc\Gamma/2\cos\alpha \approx 1$. For near-grazing incidence we replace this last term by the alternate form of g_1 obtained from (16).

Thus, up to moderately large values of α and $wc\Gamma/2\cos\alpha \not\approx 1$, we keep only the leading term of Z and use

$$R \approx [(1 - wc\Gamma/2\cos\alpha)/(1 + wc\Gamma/2\cos\alpha)]^2. \tag{25}$$

To this level of approximation, R vanishes at $\alpha = \alpha_0$, with

$$\tan\alpha_0 = (2/wc\Delta)(1 - w^2/4)^{1/2}. \tag{26}$$

At normal incidence, (25) reduces to

$$R \approx [(1 - w/2)/(1 + w/2)]^2. \tag{27}$$

For $wc\Gamma/2\cos\alpha \approx 1$, we replace (25) by

$$R \approx \left|\frac{1 - wc\Gamma/2\cos\alpha + iwe^{-2ikc\cos\alpha}/(2kc\cos\alpha)}{1 + wc\Gamma/2\cos\alpha - iwe^{-2ikc\cos\alpha}/(2kc\cos\alpha)}\right|^2. \tag{28}$$

For larger α, all the terms of Z of (24) are to be retained. As α approaches grazing, we use the first two terms of Z of (24) and the alternate form of the third term obtained from (16). Consequently, in terms of the grazing angle τ, we obtain

$$R_+ \sim 1 - 4\tau/wc\Delta, \quad R_- \sim 1 - wk^2c^3\Delta\tau\ ; \quad \tau \sim 0. \tag{29}$$

The differential scattering cross sections are given by (11) in terms of f of (8) and Z of (24). For directions of observation not near the specular and α not near grazing, we may neglect the diffracted wave contributions to f [i.e., $g_2(\hat{\mathbf{r}},\hat{\mathbf{k}})$ and $g_2(\hat{\mathbf{r}},\hat{\mathbf{k}}')$] and retain only the first term of Z. Thus

$$\sigma_{\pm} \approx \frac{wabc^2}{4\pi}\left|\frac{De^{ikP} \pm D'e^{-ikP}}{1 + wc\Gamma/2\cos\alpha}\right|^2,$$

$$(P')^2 = \mathbf{s}'\cdot\tilde{\mathbf{E}}^{-1}\cdot\mathbf{s}', \quad D' = \mathbf{s}'\cdot\mathbf{s}'/(P')^2. \tag{30}$$

The rapidly oscillating cross terms may be ignored except near grazing observation since they will not contribute significantly when integrated over a portion of the distribution or over $k\bar{a}$ (with $\bar{a}$ as the minimum semidiameter). Consequently, for both free and rigid surfaces

$$\sigma_{\pm} \approx \frac{wabc^2[D^2 + (D')^2]}{4\pi(1 + wc\Gamma/2\cos\alpha)^2}, \tag{31}$$

which drops the rapidly oscillatory terms and provides a baseline for various practical purposes.

In particular, in the back direction ($\theta = \alpha, \varphi = \pi + \beta$) for α not near normal incidence,

$$\sigma_{\pm}(b) \approx \frac{wabc^2[\delta^{-4} + (\delta^2\sin^2\alpha + c^2\cos^2\alpha)^{-2}]}{4\pi(1 + wc\Gamma/2\cos\alpha)^2}, \tag{32}$$

with $\delta^2 = (a\cos\beta)^2 + (b\sin\beta)^2$.

In the forward (specular, i.e., $\theta = \alpha, \varphi = \beta$) direction, for α not near grazing,

$$\sigma_{\pm}(f) \approx \frac{w|g_2(\hat{\mathbf{k}},\hat{\mathbf{k}})|^2}{k^2\pi ab(1 + wc\Gamma/2\cos\alpha)^2} = \frac{w\Gamma^2k^2abc^2}{4\pi(1 + wc\Gamma/2\cos\alpha)^2}. \tag{33}$$

If $\Delta^2 - 1/c^2 > 0$, the above form has a local maximum $\sigma_\wedge(f)$ at $\alpha = \alpha_\wedge$, where

$$\cos^2\alpha_\wedge = \Delta^2/[(\Delta^2 - 1/c^2) + t^{2/3}],$$

$$\sigma_\wedge(f) = \frac{wk^2abc^2\Delta^2t^{2/3}}{4\pi[(\Delta^2 - 1/c^2) + t^{2/3}]\,[1 + (wc/2)t^{1/3}]^2},$$

$$t = 2(\Delta^2 - 1/c^2)/wc. \tag{34}$$

At normal incidence, both $\sigma(f)$ and $\sigma(b)$ correspond to backscattering:

$$\sigma_{\pm}(f) = \sigma_{\pm}(b) = \frac{wk^2ab}{4\pi}\left|\frac{1 - (i/kc)e^{-2ikc}}{1 + w/2 - (iw/2kc)e^{-2ikc}}\right|^2 \approx \frac{wk^2ab}{4\pi(1 + w/2)^2}. \tag{35}$$

For α near grazing, the forward- and backscattering vanish as $O(\tau^2)$ for the rigid (+) surface and as $O(\tau^4)$ for the free (−):

$$\sigma_+(f) \sim k^2\tau^2ab/\pi w, \tag{36}$$

$$\sigma_+(b) \sim \tau^2ab/(\pi w\Delta^2\delta^4), \tag{37}$$

$$\sigma_-(f) \sim wk^6c^6ab\Delta^2\tau^4/16\pi, \tag{38}$$

$$\sigma_-(b) \sim \frac{w}{\pi}k^2ab\tau^4\left|\frac{c^3e^{-2ik\delta}}{2\delta^3} - \frac{J_1(U)}{c\Delta U}\right|^2, \tag{39}$$

where U reduces to

$$U = k|(a^2 - b^2)\sin 2\beta|/(ab\Delta).$$

IV. NUMERICAL ILLUSTRATIONS

We illustrate features of R and the forward-scattered (specular) and backscattered cross sections, $\sigma(f)$ and $\sigma(b)$ [written as $S(F)$ and $S(B)$ on the graphs to facilitate comparison with the earlier[1] normalized versions], by plots versus angle (α) from the normal for rigid (+) and free (−) surfaces. We consider both isotropic and anisotropic surfaces, and emphasize the roles of boss shape and boss orientation. For isotropic surfaces we compare results for hemispheroidal bosses of constant circular base area (πa^2) with boss height (c) as the parameter. For anisotropic surfaces,

we consider elongated ridgelike and vertical disklike bosses by using results for spheroids, as well as generalizations derived for triaxial ellipsoids. Plots versus α with azimuthal angle β as the parameter (such that $\beta = 0°$ corresponds to broadside incidence at grazing, and $\beta = 90°$ to nose-on) exhibit the effect of surface anisotropy. For the triaxial case, we fix the boss volume (and height and base area) but vary the ratio of the base diameters to separate shape effects from volume effects.

For all cases, we take $k\bar{a} = 20$ (with $2\bar{a}$ as the smallest diameter) and $w = 0.2$ (and discount correlations). In the figures, curves for the rigid surfaces are shown solid and curves for the free surfaces are dotted. Curves obtained from Eqs. (25), (32), and (33) are shown dashed; these serve as baselines for the oscillations of R, $\sigma(b)$, and $\sigma(f)$, respectively, arising from interference of the wave components in the more complete expressions. Computations with the explicit approximations of (13) based on (14)–(18) suffice in general. However, in calculating R we use the uniform integral approximation (13) for g_1 to avoid switching from (14) to (15) for α near grazing; computations based on g_1 of (14) gave unrealistically high values for R_- near grazing for some values of the parameters.

Figures 1–3 correspond to isotropic distributions. Figure 1 compares R for hemispheroids with fixed circular base

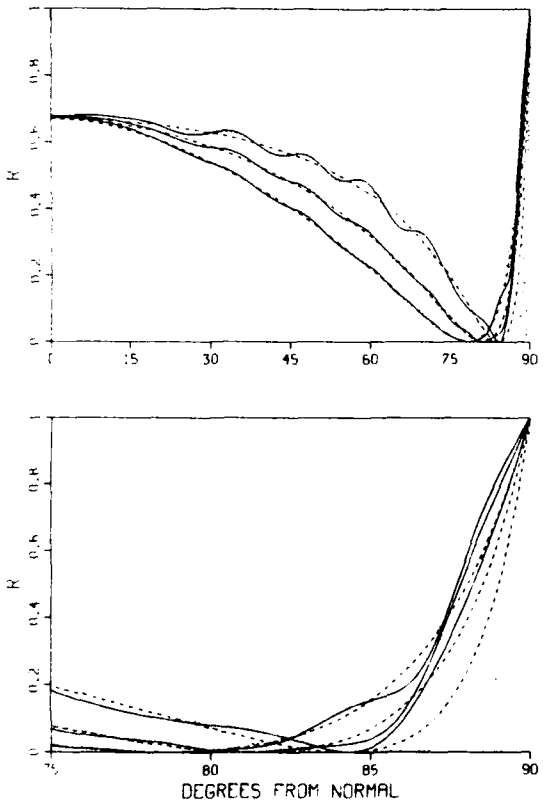

FIG. 1. Graphs of the reflection coefficient R of (10) for hemispheroidal bosses of fixed base radius $a = 2$ and height c as the parameter. The solid and dotted curves obtained from (24) correspond to rigid (+) and free (−) surfaces, respectively; the dashed baseline curves were obtained from (25). The upper panel shows the full range of angle of incidence (α), while the lower shows the near-grazing region. The lower curves for α not near 90° apply for the larger values of $c = 2,3,4$.

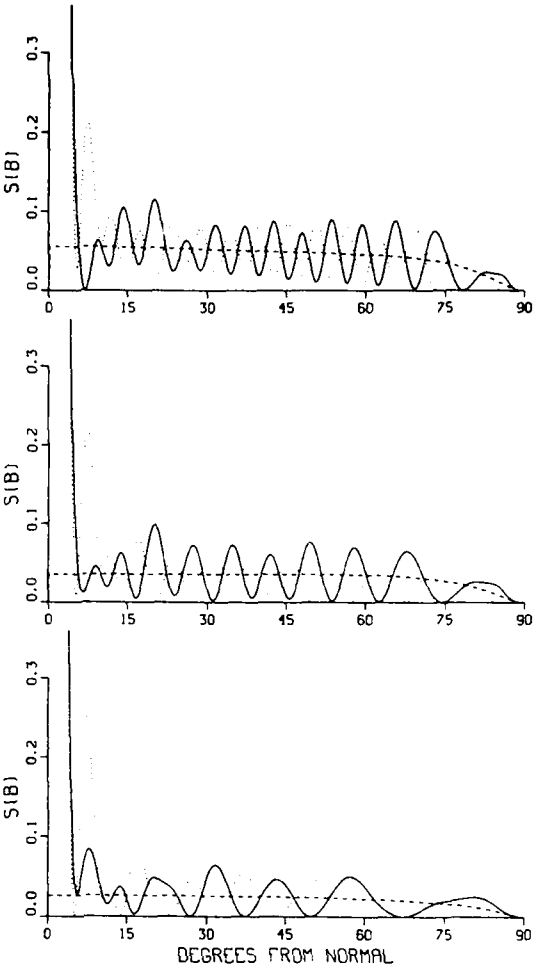

FIG. 2. The backscattering curves from (11) and dashed bases from (32) associated with R of Fig. 1. The upper, center, and lower panels correspond to $c = 4$, 3, and 2, respectively.

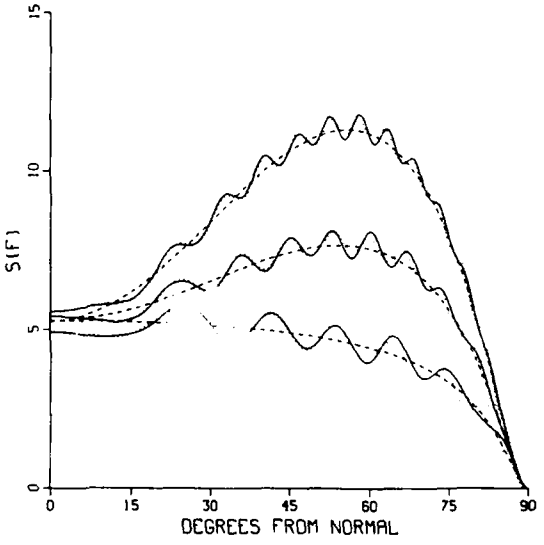

FIG. 3. The forward scattering from (11) and dashed bases from (33) associated with R of Fig. 1. The higher curves apply for the larger values of $c = 4,3,2$.

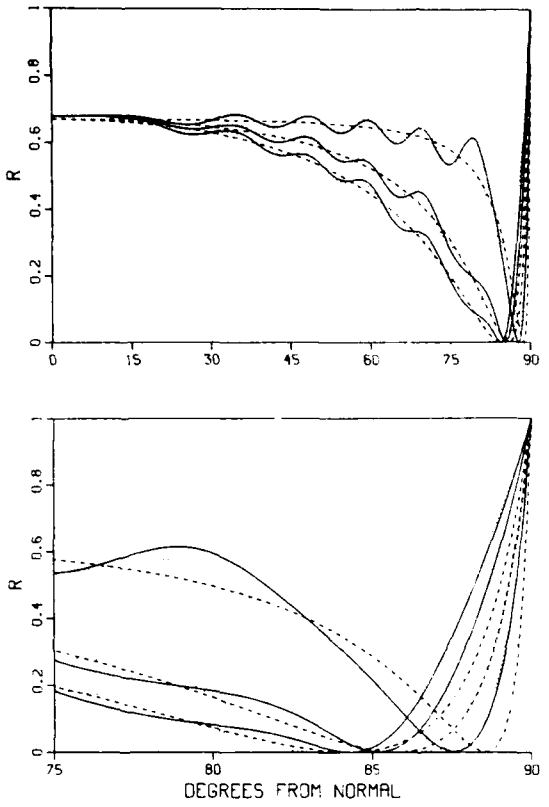

FIG. 4. Graphs of R for elongated ridgelike bosses $(a,b,c) = (1,4,1)$ with azimuthal angle β as parameter. The higher curves for α not near 90° correspond to the larger values of $\beta = 90°$, 45°, and 0° (with 0° as broadside incidence at grazing).

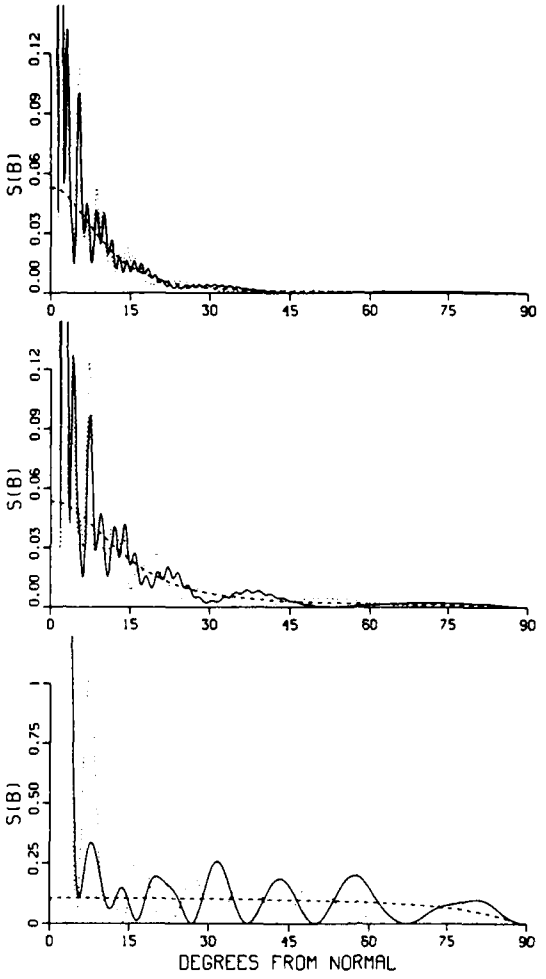

FIG. 5. The backscattering curves associated with Fig. 4. The top, center, and lower panels correspond to $\beta = 90°$, 45°, and 0°, respectively.

(of radius $a = 2$) and boss height ($c = 2,3,4$) as the parameter. The associated backscattering and forward scattering are shown in Figs. 2 and 3. Scattering effects increase as the boss height (and scatterer volume) increases. To the present level of approximation, the R baseline curves in Fig. 1 show zeros (shifted to smaller α with increasing c) corresponding to (26), and the forward-scattering baseline curves in Fig. 3 show maxima whose location and magnitude are determined by (34).

Plots for anisotropic distributions of aligned elongated ridgelike bosses or vertical disklike bosses, as well as triaxial generalizations, are shown in Figs. 4–12. The dependence on azimuthal angle is illustrated in Figs. 4–9, where we take β as the parameter. The essentials are indicated by the simple approximations (25), (32), and (33) through their dependence on $\Delta(\beta)$ and $\delta(\beta)$. For ridgelike bosses $(a,b,c) = (1,4,1)$ as in Figs. 4–6, Δ decreases from 1 to $\frac{1}{4}$ as β increases from 0° to 90°, while δ increases from 1 to 4. Thus, for moderate α, R of Fig. 4 increases with increasing β as indicated by the baseline form (35). The trend is maintained at near grazing for the free surface and reversed for the rigid; see Eq. (29). The zero of R_+ is shifted to larger values of α with increasing β as indicated by (26), as is the minimum of R_-. Similarly, the baseline curves for the back- and forward scattering in Figs. 5 and 6 are higher for $\beta = 0°$ (broadside incidence) than for $\beta = 90°$ (nose-on). Analogous plots of R, $\sigma(b)$, and $\sigma(f)$ for vertical disklike bosses $(a,b,c) = (1,4,4)$ are shown in Figs. 7–9.

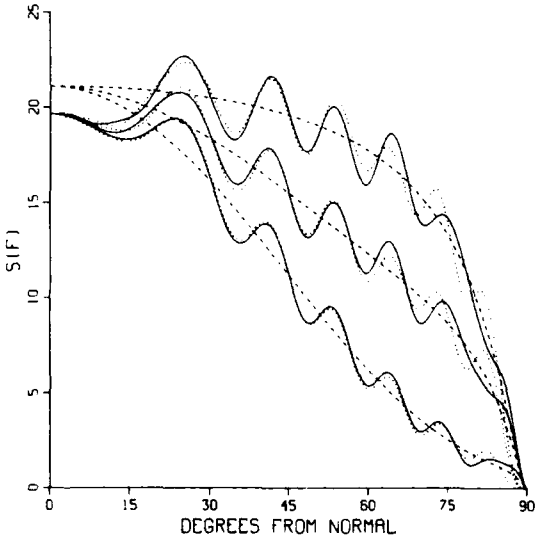

FIG. 6. The forward-scattering curves associated with Fig. 4. The higher curves correspond to the smaller values of $\beta = 0°$, 45°, and 90°.

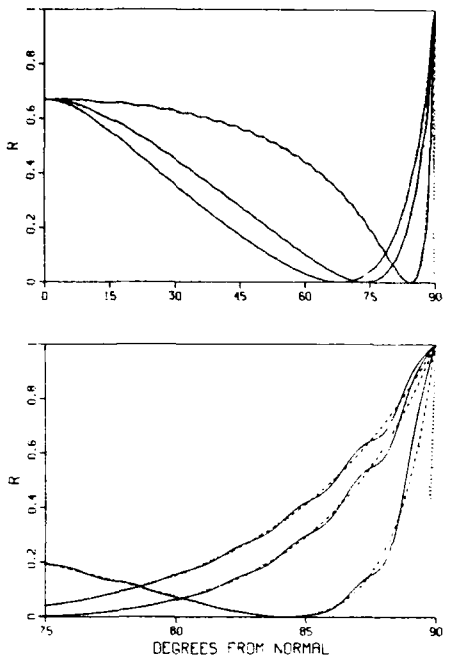

FIG. 7. Plots of R for vertical disklike bosses $(a,b,c) = (1,4,4)$ with azimuthal angle β as the parameter. The higher curves for α not near 90° correspond to the larger values of $\beta = 90°$, 45°, and 0°.

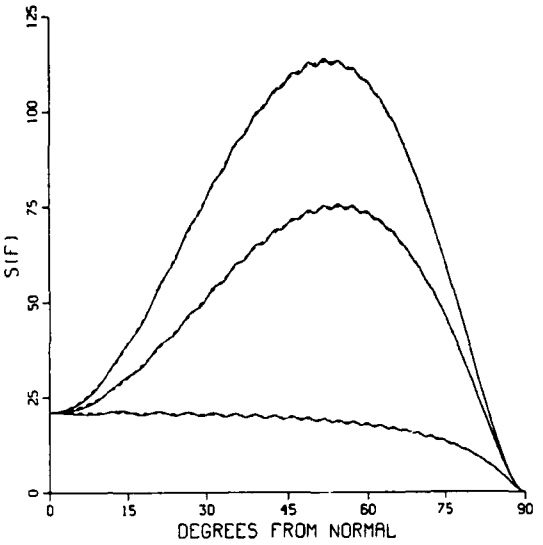

FIG. 9. The forward-scattering curves associated with Fig. 7. The higher curves correspond to the smaller values of $\beta = 0°$, 45°, and 90°.

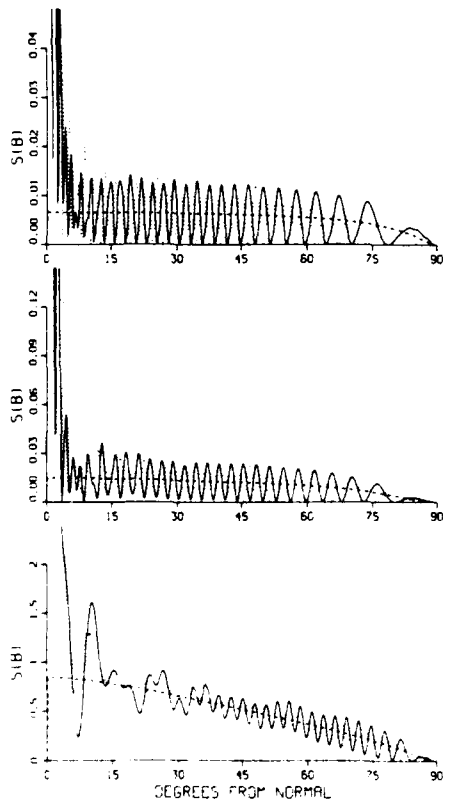

FIG. 8. The backscattering curves associated with Fig. 7. The top, center, and lower panels correspond to $\beta = 90°$, 45°, and 0°, respectively

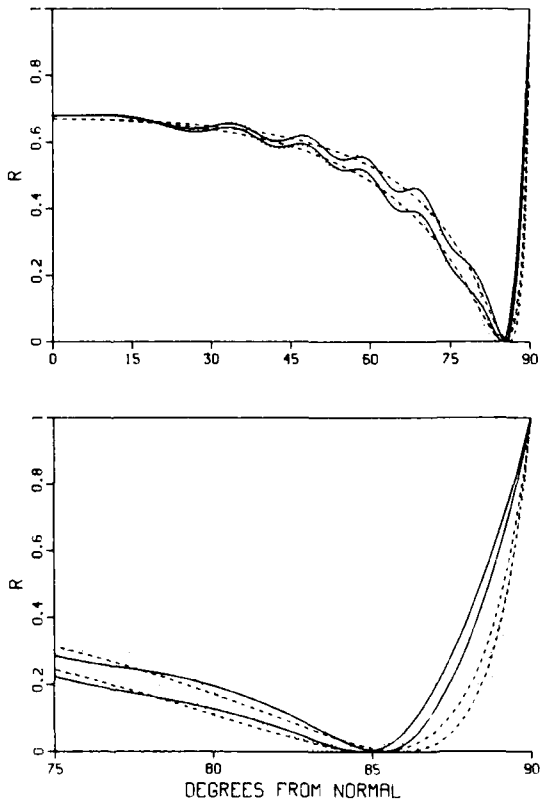

FIG. 10. Graphs of R for triaxial bosses with height $c = 1$ and constant base area $\pi ab = \pi a^2 t = \pi 4$, with t as the parameter, i.e., for fixed boss volume. The higher curves for α not near 90° correspond to $t = 2$ and the lower curves to $t = 3$.

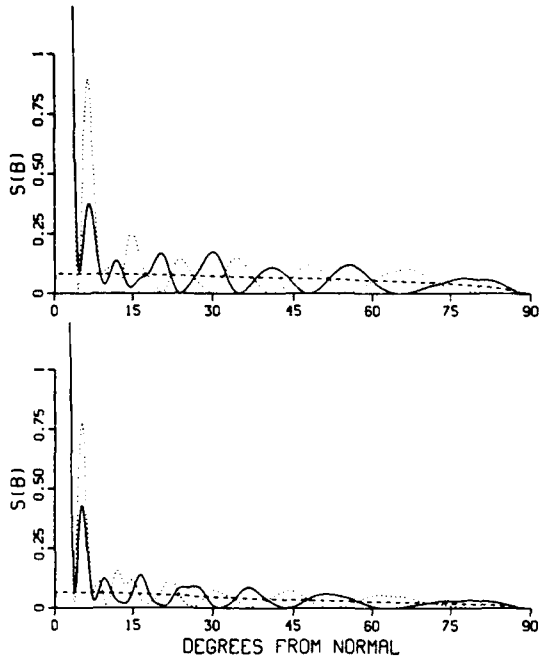

FIG. 11. The backscattering curves associated with Fig. 10. The upper panel corresponds to $t = 3$ and the lower to $t = 2$.

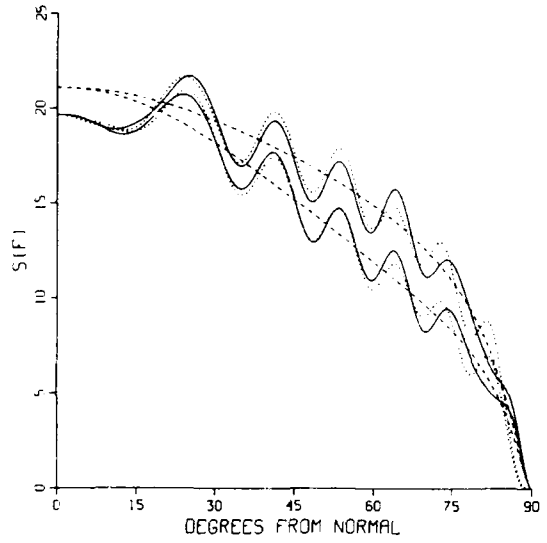

FIG. 12. The forward-scattering curves associated with Fig. 10. The higher curves correspond to $t = 3$ and the lower to $t = 2$.

Figures 10–12 for $c = 1$ and $ab = a^2t = 4$ with $t = 2,3$ serve to separate shape and volume effects. The bosses for the two cases have the same volume and base area, but differ in the ratio of the base diameters a/b.

ACKNOWLEDGMENTS

Work supported in part by the Office of Naval Research and the National Science Foundation.

[1]R. J. Lucas and V. Twersky, "Low-frequency reflection and scattering by ellipsoidally embossed surfaces," J. Acoust. Soc. Am. **78**, 1838–1850 (1985).

[2]V. Twersky, "On scattering and reflection of sound by rough surfaces," J. Acoust. Soc. Am. **29**, 209–225 (1957).

[3]V. Twersky, "Reflection and scattering of sound by correlated rough surfaces," J. Acoust. Soc. Am. **73**, 85–94 (1983).

[4]J. E. Burke and V. Twersky, "Elementary results for scattering by large ellipsoids," J. Acoust. Soc. Am. **38**, 589–598 (1965).

[5]Lord Rayleigh, "On the light dispersed from lines ruled upon reflecting surfaces or transmitted by very narrow slits," Philos. Mag. **14**, 350–359 (1907).

[6]J. E. Burke and V. Twersky, "Scattering and reflection by elliptically striated surfaces," J. Acoust. Soc. Am. **40**, 883–895 (1966).

[7]O. I. Diachok, "Effect of sea-ice ridges on sound propogation in the ocean," J. Acoust. Soc. Am. **59**, 1110–1120 (1976); T. McClanahan and O. Diachok, "Ultrasonic modeling of acoustic scattering from striated surfaces depicting the Artic Ocean ice cover," J. Acoust. Soc. Am. Suppl. 1 **76**, S54 (1984); S. Wales and O. Diachok, "Incorporating the Burke–Twersky reflection model into the fast field program to predict under-ice transmission loss," J. Acoust. Soc. Am. Suppl. 1 **76**, S86 (1984); E. Livingston and O. Diachok, "Extraction of average under-ice reflection amplitudes and phases with matched field processing," J. Acoust. Soc. Am. Suppl. 1 **81**, S85 (1987).

[8]W. I. Roderick and R. K. Dullea, "High resolution bottom back scatter measurements," NUSC Tech. Doc. 7181, Naval Underwater Systems Center, New London, CT, 1984; W. I. Roderick, "Sea surface forward scatter and reverberation measurements using parametric arrays, J. Acoust. Soc. Am. Suppl. 1 **76**, S78 (1984); W. I. Roderick, R. K. Dullea, and J. M. Syck, "High resolution bottom back scatter measurements," J. Acoust. Soc. Am. Suppl. 1 **75**, S31 (1984); W. I. Roderick, R. K. Dullea, and J. B. Chester, "High-frequency acoustic back scatter from the sea surface," J. Acoust. Soc. Am. Suppl. 1 **75**, S31 (1984).

[9]C. E. Weatherburn, *Advanced Vector Analysis* (Bell, London, 1949).

[10]W. H. McCrea, *Analytic Geometry of Three Dimensions* (Oliver and Boyd, Edinburgh, 1953), pp. 106–109.